Temperature and Pressure Dependence of Polystyrene Dynamics through Molecular Dynamics Simulations and Experiments

ARTICLE *in* MACROMOLECULES · JANUARY 2011

Impact Factor: 5.8 · DOI: 10.1021/ma102179b · Source: OAI

3 AUTHORS, INCLUDING:

V. A. Harmandaris
University of Crete
59 PUBLICATIONS **1,900** CITATIONS

SEE PROFILE

George Floudas
University of Ioannina
229 PUBLICATIONS **4,182** CITATIONS

SEE PROFILE

Macromolecules
ARTICLE

Macromolecules **2011**, *44*, 393–402 **393**
DOI: 10.1021/ma102179b

Temperature and Pressure Dependence of Polystyrene Dynamics through Molecular Dynamics Simulations and Experiments

Vagelis A. Harmandaris,*,†,‡,∥ George Floudas,*,§,⊥ and Kurt Kremer∥

†*Department of Applied Mathematics, University of Crete, GR-71110 Heraklion, Greece,* ‡*IACM FORTH, GR-71110 Heraklion, Greece,* §*Department of Physics, University of Ioannina, GR-45110, Ioannina, Greece,* ⊥*Foundation for Research and Technology-Biomedical Research Institute, Ioannina, Greece, and* ∥*Max Planck Institute for Polymer Research, D-55128 Mainz, Germany*

Received September 21, 2010; Revised Manuscript Received December 9, 2010

ABSTRACT: We present a detailed comparison of the segmental and chain dynamics of an atactic monodisperse polystyrene (molecular weight 1800 g/mol) (a-PS) studied by hierarchical multiscale molecular dynamics (MD) simulations, with an atactic polystyrene (M_n = 1644 g/mol, polydispersity index 1.14) investigated by dielectric spectroscopy, rheology and differential scanning calorimetry. The MD simulations, performed at three temperatures (403, 433, and 463 K), can capture the temperature dependence of the segmental and terminal relaxations in good quantitative agreement with experiment, taking into account the uncertainties in the development of the atomistic force field. In addition, ring and backbone segmental dynamics are studied by analyzing time-correlation functions for various bond vectors in the monomer level. MD simulations at elevated pressures (40 and 60 MPa) were also in good agreement with experiments probing the pressure-dependent glass temperature.

1. Introduction

Accurate knowledge of the local and global polymer dynamics[1,2] as a function of temperature and pressure is important for technological applications, since they dictate the processability and the final mechanical and electrical properties of polymers. Therefore, efforts to obtain and ultimately predict these properties, either through experimental methods or theoretical and simulation approaches, have attracted considerable interest over the years.[1−5]

Recent experimental efforts have addressed the origin of the freezing of the dynamics at the liquid-to-glass temperature by decreasing temperature or increasing pressure. One such approach emphasized the importance of monomer volume and local packing[6] whereas other approaches proposed[7−11] a thermodynamic scaling of the dynamics on temperature and density. Of central importance in these experimental efforts has been the application of pressure, since it can be applied isothermally, thus affecting only the density.

In addition to experiments molecular dynamics (MD) simulations provide an excellent tool for investigating polymer dynamics as a function of temperature and pressure at various length scales. Thus, over the past years, several attempts have been made to exploit MD trajectories for simplified generic, coarse grained or even atomistic models and calculate relaxation times both at the segmental and at the end-to-end distance level.[12−31] In MD the segmental dynamics is usually studied through the time-decay of autocorrelation functions of various quantities, such as dihedral angles, dipolar moments, C−H bond vectors which then can be directly compared with experimental probes (NMR, dielectric spectroscopy (DS)).

Boyd and collaborators[12,13] were the first to report simulation results for the effect of pressure, and temperature, on the thermodynamic and structural properties of polyethylene (PE) by performing MD runs. They studied a single PE chain, which folded back into the original box via periodic boundary conditions in order to reach melt density. Other simulation studies of pressure effects on the dynamics of amorphous polymers include the MD works of Hotston et al.[14] and Smith and co-workers[15,16] on the segmental relaxation of PE and 1,4-polybutadiene (PB) respectively, and of Yang et al.[17] on the glass transition of a model polymer through isobaric or isochoric cooling. Segmental dynamics at ambient atmospheric pressure of different polymers have also been exploited through atomistic MD simulations. These studies include the local structure and the local reorientation dynamics of C−H bonds in *trans*-polyisoprene oligomers,[25] the local dynamics of a miscible blend of *cis*-1,4-PI with 1,2-PB,[24] and the dynamics of atactic polypropylene.[21] In addition to temperature, pressure effects on the structure and dynamics were studied in *cis*-1−4 PB.[22]

Atactic polystyrene has also been investigated by simulations. The segmental dynamics in atactic polystyrene with molecular weight of 2200 g/mol was recently studied by MD simulations at three temperatures and the results were compared with NMR spin−lattice relaxation experiments.[17] The simulated segmental relaxation times were slower by a factor of 1.8, however the comparison indicated a qualitative agreement of the shape of the $P_2(t)$ orientation autocorrelation function as probed by MD and experiments. In addition, united atom MD simulations have addressed the segmental dynamics and the issue of dynamic heterogeneity near the glass transition temperature for short atactic polystyrene chains.[26,27]

With MD simulations usually only oligomeric systems (i.e., low molecular weight polymers) can be investigated in all-atom detail and, even then, for a rather limited range of temperatures and pressures. The reason are difficulties arising from the wide spectrum of time- and length-scales characterizing their structure and associated dynamics. To overcome these difficulties, coarse grained (CG) dynamic simulations have been developed. Such CG MD simulations are capable of exploiting a broader range of

*Corresponding authors. E-mail: (V.A.H.) vagelis@tem.uoc.gr; (G.F.) gfloudas@cc.uoi.gr.

Published on Web 12/27/2010

time- and length-scales due to the simpler models and bead interactions as compared to the more detailed all-atom ones. For this purpose various coarse-grained models have been used in studying the dynamics of bulk polymers, varying from simple bead−spring models[29−31] to more detailed, systematically obtained CG models, that allow a quantitative study of the structure and dynamics of specific polymeric systems (see, for example, refs 4, 5, 29, and 32−35 and references within).

Despite recent progress made with the aid of various MD simulation methods and experiments, an in-depth understanding of the molecular mechanisms governing the (multiple) relaxation processes of polymers, is still lacking. In particular, a comparison of the local segmental and chain dynamics as deduced from simulations and experiments at temperatures and pressures that are typically encountered during processing is a necessity for understanding—and ultimately predicting—properties of polymers. Multiscale simulation approaches combined with experimental methods with the capability of probing the dynamics at the molecular level are best suited for this purpose.

Here we present such a methodology that combines systematic multiscale simulation methods and experimental techniques for understanding the dynamics of atactic polystyrene (a-PS). The polymer dynamics is examined both at the submonomer and end-to-end distance level. At the same time the temperature and the pressure dependence of the segmental dynamics is studied and compared with the results from dielectric spectroscopy, rheology and differential scanning calorimetry made on the very same sample. In addition, the results of the equation-of-state, obtained from pressure-volume-temperature measurements, are employed as a guide for the MD simulations. Overall the main goal of the present work is to provide a direct comparison of the segmental and terminal dynamics from simulation and experiments (DS, rheology) at atmospheric pressure and, for the first time, of the segmental dynamics at elevated pressures. The paper is organized as follows. In the first two sections, a brief overview of the experimental techniques as well as of the atomistic and the coarse-grained simulations is given. Results on the relevant thermodynamic properties and comparison of the dynamics as probed by MD simulations and experiments are presented in section 4. Finally, our findings and conclusions are summarized in section 5.

2. Experimental Methods

2.1. Sample. The PS sample, synthesized by J. Thiel in Mainz, had $M_w = 1870$ g/mol, $M_n = 1644$ g/mol giving a polydispesrity of $M_w/M_n = 1.14$. The glass temperature was at 334 K as determined by differential scanning calorimetry (DSC) at a heating rate of 10 K/min (from the second heating circle) with a heat capacity step, Δc_p, of $\Delta c_p = 0.32$ J/gK.

2.2. Pressure−Volume−Temperature (*PVT*). Pressure−volume−temperature measurements were made using a fully automated GNOMIX high-pressure dilatometer. About 1 g was used in the measurements. First, we performed runs by changing pressures from 10 to 200 MPa in steps of 10 MPa at constant temperatures (i.e., under "isothermal" conditions) from 293 to 433 K. Subsequently, measurements were made by heating/cooling experiments with a rate of 1 K/min at different fixed pressures (i.e., under "isobaric" conditions) in the range from 10 to 200 MPa. The 0.1 MPa data were obtained by extrapolation from the higher pressures. The data from the "isothermal" measurements are shown in Figure 1 for the different pressures. The $V(P,T)$ data can be parametrized according to the Tait equation

$$V(P,T) = V(0,T)\left\{1 - 0.0894 \ln\left[1 + \frac{P}{B(T)}\right]\right\} \qquad (1)$$

where, $V(0,T) = (0.8165 + 4.5 \times 10^{-4}T)$ (V in cm^3/g, T in K) is the specific volume at atmospheric pressure and $B(T) = (446\ \text{MPa})\exp(-0.00029T)$ (T in K) are the parameters in the liquid melt state. In the glassy state, the following parameters were employed: $V(0,T) = (0.9486 + 5 \times 10^{-5}T)$ (V in cm^3/g, T in K) and $B(T) = (212.5\ \text{MPa})\exp(0.00046T)$ (T in K). The glass temperature, at each pressure, was determined by extrapolating the $V(P)$ dependencies below and above the "transition" and the resulted glass temperatures (T_g) are plotted as an inset to Figure 1.

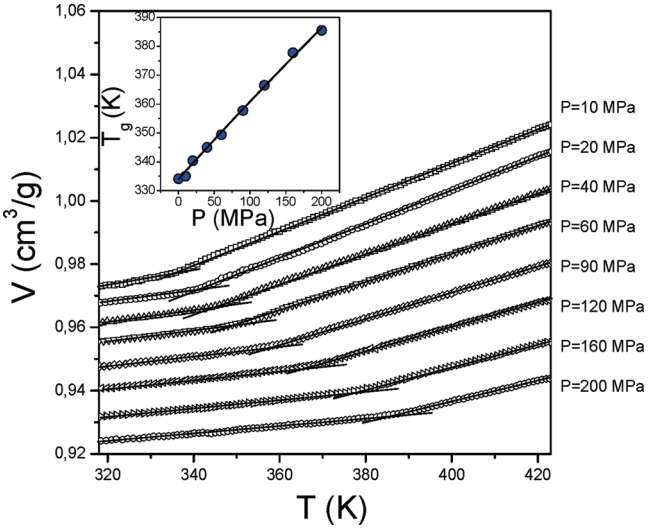

Figure 1. Specific volume as a function of temperature for different pressures in the range from 10 to 200 MPa, obtained from *PVT* measurements. The lines represent linear fits to temperatures below and above the liquid-to-glass temperature and the latter is obtained from their intersection. Inset: Glass temperature as a function of pressure. The line is a fit to eq 5.

2.3. Dielectric Spectroscopy (DS). Dielectric measurements were made under isobaric (atmospheric pressure) conditions as a function of temperature at different temperatures in the range 123.15−423.15 K and for frequencies in the range from 10^{-2} to 10^6 Hz. The complex dielectric permittivity $\varepsilon^* = \varepsilon' - i\varepsilon''$, where ε' is the real and ε'' is the imaginary part, was obtained as a function of frequency ω and temperature T, i.e., $\varepsilon^*(T,\omega)$.[36] The analysis of the T- dependent experiments was made using the empirical equation of Havriliak and Negami (HN):

$$\varepsilon^*(T,P,\omega) = \varepsilon_\infty(T,P) + \frac{\Delta\varepsilon(T,P)}{[1 + (i\omega\tau_{HN}(T,P))^m]^n} + \frac{\sigma_0(T,P)}{i\varepsilon_f\omega} \qquad (2)$$

where $\varepsilon_\infty(T)$ is the high frequency permittivity, $\tau_{HN}(T)$ is the characteristic relaxation time in this equation, $\Delta\varepsilon(T) = \varepsilon_o(T) - \varepsilon_\infty(T)$ is the relaxation strength, m, n (with limits $0 < m, mn \le 1$) describe, respectively, the symmetrical and asymmetrical broadening of the distribution of relaxation times, σ_o is the dc-conductivity and ε_f is the permittivity of free space. From τ_{HN}, the relaxation time at maximum loss, τ_{max}, is obtained analytically following

$$\tau_{max} = \tau_{HN}\left[\frac{\sin\left(\frac{\pi m}{2+2n}\right)}{\sin\left(\frac{\pi mn}{2+2n}\right)}\right]^{-1/m} \qquad (3)$$

Some representative dielectric loss spectra are shown in Figure S1 of the Supporting Information. In DS, the quantity that is probed is the fluctuation of the weak dipole moment associated with styrene (∼0.12 D) with a direction perpendicular to the backbone.[36] Subsequently, the DS spectra (Figure S1, Supporting Information) were analyzed using eq 2 and the relaxation times at maximum loss were extracted. From the

shape parameters m and n, the single Kohlrausch−Williams−Watts (KWW) exponent β was obtained following[37] $\beta = [mn]^{1/1.23}$, that is based on the following constraint on m and n: $n = 1 - 0.812(1 - m)^{0.387}$.

2.4. Rheology. An advanced rheometric expansion system (ARES) equipped with a force-rebalanced transducer was used in the oscillatory mode. Depending on the temperature range two transducers were used with 2000, 2 g·cm and 200, 0.2 g·cm upper and lower sensitivity, respectively. The sample was prepared on the lower plate of the 10 mm diameter parallel plate geometry setup and heated under a nitrogen atmosphere until it could flow. Subsequently, the upper plate was brought into contact, the gap thickness was adjusted to 1 mm, and the sample was slowly cooled to the desired starting temperature. For the lower temperatures investigated (near the glass temperature) plates with 6 mm diameter were employed. The storage (G′) and loss (G″) shear moduli were monitored in different types of experiments. These experiments involved isothermal frequency scans for temperatures in the range 329−373 K and for frequencies $10^{-1} < \omega < 10^{2}$ rad/s. In Figure S2 of the Supporting Information, a master-curve of the storage and loss moduli is shown. According to the principle of time−temperature superposition (tTs), the frequency (ω) dependence of the complex shear modulus G^* at any temperature can be obtained from a master curve at a reference temperature (T_r) according to $G^*(\omega,T) = G^*(a_T\omega; T_r)$. According to t$T$s, at each temperature a single frequency-scale shift factor a_T allows superposition of all modulus data at temperature T to the corresponding data at T_r. The horizontal shift factors can be described by the Williams−Landel−Ferry (WLF) equation[1]

$$\log_{10} a_T = -\frac{c_1{}^r(T - T_r)}{c_2{}^r + (T - T_r)} \quad (4)$$

where $c_1{}^r$ (=14.8) and $c_2{}^r$ (=69.4 K) are the WLF parameters at the reference temperature (T_r = 332.15 K). These values, when calculated at T_g (=334 K), result to $c_1{}^g$ = 14.4 and $c_2{}^g$ = 71.4 K. When these shift factors apply to the segmental and terminal relaxations, they provide us with the full T-dependence.

3. Molecular Simulations

The hierarchical simulation approach presented here involves detailed all-atom (AA) and coarse-grained (CG) MD simulations of an atactic PS melt with M = 1800 g/mol, i.e., with a molecular weight close to the experimental conditions.

3.1. Atomistic Simulations. An important goal of the present work is the investigation of segmental and chain dynamics of PS, at the all-atom detail, as a function of both temperature and pressure aiming at a comparison with the experimental results from dielectric spectroscopy (DS), differential scanning calorimetry (DSC) and PVT measurements, the latter performed on the same sample. To achieve this, all-atom MD simulations of short PS chains were performed using a model, where hydrogens and carbons are treated explicitly.[38] All bond lengths were kept rigid whereas a harmonic potential was used to describe bond angle bending. Standard torsional potentials were used to describe rotations along bonds in the aliphatic backbone. Parameters of the barriers for the rotation of polystyrene backbone dihedral angles were calculated from ab initio calculations on polystyrene fragments. Nonbonded interactions were described by pairwise-additive Lennard-Jones potentials. Furthermore, the AA model included partial charges on the carbon and hydrogen atoms of the phenyl groups that reproduce the electric quadropole moment of the benzene molecule. For more details of the model see ref 38.

Using this AA model, atomistic MD simulations of an atactic PS melt of 36 chains with molecular weight, M = 1800 g/mol (18mer), were performed for a range of temperatures and pressures. The molecular dynamics package

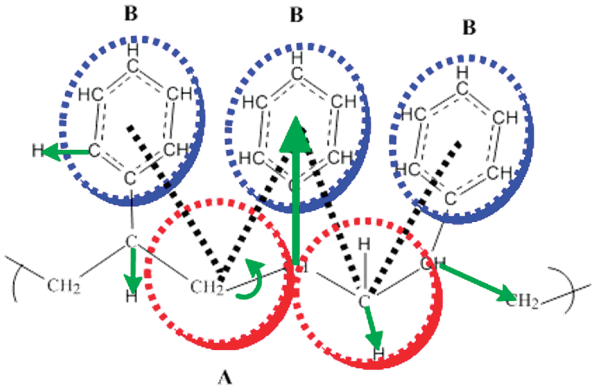

Figure 2. Atomistic and coarse grained model of PS chain. In the CG model one monomer is mapped to two different CG beads (σ_A = 4.1 Å, m_A = 27 amu; σ_B = 5.2 Å, m_B = 77 amu). Dashed lines show CG bonds between CG beads A and B. The arrows indicate the different vectors where the time−autocorrelation functions were calculated.

GROMACS[39] was employed for the atomistic MD simulations. Initial well-equilibrated atomistic configurations were obtained by back-mapping of the CG melts.[32,33] All-atom MD simulations were conducted under constant temperature and volume NVT conditions using the Berendsen thermostat (coupling time 0.1ps).[39] As a guide for the densities of the simulated melt we employed the experimental PVT data depicted in Figure 1. We should also note here, that pressure in the atomistic simulations is slightly negative (by about 10−20 MPa) since the density predicted by the AA force-field is about 3−4% larger than the experimental ones. A negative pressure, induced by the constant volume constraint, is unphysical and would lead to inhomogeneities in the system. However, this is not the case here because the fluctuations of instantaneous pressure due to the small system size are about 5−10 times larger than the average (negative) pressure. In addition, runs at higher than atmospheric pressure were made under NVT conditions at densities corresponding to the experimental densities at the specific pressure (Figure 1). In all cases the pressure of the atomistic simulations is slightly smaller than the experimental one. Nonbonded interactions were cutoff beyond 1.2 nm. Tail corrections for the energy and pressure were applied. The integration time step was 1 fs. Finally, the overall atomistic simulation time of the production runs ranged from 0.5 to 2 μs depending on the actual temperature and pressure. All segmental relaxation times, reported in the present work, were calculated by analyzing these all-atom MD simulations.

3.2. Coarse-Grained Simulations of Polystyrene. The CG MD simulations have been performed using a model where one PS monomer is mapped onto two effective coarse-grained beads.[33] In this model a CG bead "A" includes information from 3 consequent CH_x groups along the backbone (see Figure 2). In more detail, CG bead "A" corresponds to the CH_2 of a PS monomer plus the half mass of each of the two neighboring CH groups along the chain backbone, whereas CG bead "B" is just the phenyl ring. This model has the advantage of capturing tacticity without introducing side groups. More details about the CG model and the procedure to obtain the CG force-field can be found elsewhere.[32−35,40]

All coarse-grained MD simulations were performed using the ESPResSO package.[41] PS melts of 100 chains were simulated. The size of the box is fixed such that the density of the PS melt is equal to that of the experimental density. Periodic boundary conditions were used. Also, CG MD simulations have been performed in dimensionless LJ units using m_A to

scale all masses, σ_{AV} [$\sigma_{AV} = (\sigma_A + \sigma_B)/2$] to scale all lengths and ε ($\varepsilon = kT$) to scale all energies. The time step used in the MD simulations was $dt = 0.01\tau$, where τ is defined as $\tau = (m\sigma^2/\varepsilon)^{1/2}$. In order to control the temperature in the system a Langevin thermostat was employed with friction coefficient $\Gamma = 1.0\tau^{-1}$. MD simulations were performed for times 1×10^4 to $1 \times 10^5\tau$ depending upon the actual temperature and pressure. Note that even though τ has the unit of time, it is the physical time of the coarse grained model, rather than that of the underlying polymer with its specific chemical structure and has to be scaled accordingly.[32,34] The main reason for that is the softer interaction in the CG models compared to the all atom models. Calibration of the CG time scale with respect to the atomistic simulations will be discussed below. Note that the CG model used here has been parametrized at $T = 463$ K. However, various tests have shown that it can be used in a $\pm 15-20\%$ range of temperatures without any loss of accuracy.[33,35]

Finally, we should state that, as mentioned above, the CG MD simulations in this work were used: (a) for equilibrating the PS melts in the CG description, thus providing, through a back-mapping procedure, initial well-equilibrated all-atom configurations, and (b) for probing chain (end-to-end distance) relaxation of PS melts, which cannot be calculated from the all-atom MD simulations because of the very long relaxation times.

4. Results and Discussion

4.1. Thermodynamics. First we present $V(P,T)$ data from PVT measurements in Figure 1. From these data the glass temperature was extracted at each pressure and the resulting $T_g(P)$ can be described by the following empirical equation

$$T_g(P) = T_g(0)\left(1 + \frac{\kappa}{\lambda} P\right)^{1/\kappa} \quad (5)$$

where $T_g(0)$ is the glass temperature at 0.1 MPa (334 K) and κ and λ are system-specific parameters that amount to 1.72 ± 0.8 and 1210 ± 60 MPa, respectively. The initial slope, $(dT_g/dP)_{P\to 0}$ amounts to 0.277 K/MPa, i.e., similar to earlier reports for PS.[11,42] Equation 5 was first proposed for the melting of solidified gases under pressure,[43] and subsequently, it was employed by others to describe the pressure dependence of the glass temperature in glass-forming systems.[44,45]

4.2. Analysis of the MD Simulations. In the following, we will first discuss the experimental and MD results for the segmental and chain dynamics at *atmospheric pressure*. We examine the segmental dynamics of the atactic PS melt, as predicted from all-atom MD simulations, by analyzing autocorrelation functions of different vectors that include the C−CM ring and C−H bond vectors as shown in Figure 2. To examine the difference between the relaxation along the backbone and in the ring we also distinguish the C−H vectors along the backbone and in the ring.

In MD simulations different measures of the segmental dynamics of polymer melts can be employed. For example, a very common measure is by calculating time-correlation functions of a vector, $\mathbf{v}_b$, representing a chemical bond. The reorientation of such a vector can be studied by considering ensemble-averaged Legendre polynomial of order l, $P_l(t)$, of the inner product of the unit vector parallel to $\mathbf{v}_b$ at time $t = t$ and $t = 0$. A common choice for the vector $\mathbf{v}_b$, if someone is interested to compare with NMR data, is the C−H vector. The reason is that for ^{2}H nuclei, spin−lattice relaxation is dominated by electric quadrupole coupling and the spin relaxation time can be directly related to the reorientation of the C−^{2}H bond. In this case, the second Legendre polynomial: $P_2(t) = {}^3/_2\langle\cos^2(\theta(t))\rangle - {}^1/_2$, where $\theta(t)$ is the angle of $\mathbf{v}_b$ bond at time t relative to its original position is employed as a measure of the polymer segmental dynamics, and $\langle ... \rangle$ denotes the ensemble average over all chains in the system. If, on the other hand, a comparison with DS is sought (as in the present case), then a more suitable vector $\mathbf{v}_b$, is one starting from the backbone CH to the center of mass (CM) of the phenyl ring (shown by a thick arrow in Figure 2). In this case the quantity of interest is the first Legendre polynomial: $P_1(t) = \langle\cos(\theta(t))\rangle$. In addition, MD can provide the correlation functions of various other vectors, such as the C−C backbone vector, the α C−H, the β C−H, and the ring C−H as well as the dihedral angle (see Figure 2). All these correlation times can, in principle, be compared to the experimentally obtained ones. Simulations also offer the opportunity to study cross-correlations. However, there we do not know of currently available experimental data to compare to.

As an example, Figure 3a compares the $P_2(t)$ autocorrelation curves of various C−H bond vectors as well as the C−CM ring vector at the same temperature and pressure conditions ($T = 433$ K, $P = 0.1$ MPa). $P_2(t)$ exhibits a rapid decay at short times (shorter than about 10−100 ps) followed by a rather slow decorrelation at later times. The short-time regime (not shown here) corresponds to a primitive (bond vibrations and angle librations) relaxation, whereas the long-time regime corresponds to the segmental (α-) relaxation. All curves, for the range of temperatures and pressures studied here, show the same structure that is typical for amorphous polymer.[13,16,22] At a first glance, clearly the slower decay corresponds to the C−C backbone vector followed by the C−CM ring whereas the ring C−H is the fastest. This is not surprising given that C−H bonds on the phenyl ring can relax due to the motion of the backbone but also due to the faster rotational dynamics (reorientation) of the ring. Similar conclusion has been reported in the past by Vorselaars et al. in a detailed analysis of the phenyl-ring motions of PS near T_g using united-atom MD simulations.[27]

Another important aspect is related to the relaxation of the PS backbone at the monomer level and the effect of the side group. To examine this we further distinguish C−H bonds along the backbone, i.e., C−H bonds at the α C (where the phenyl group is attached) and the two C−H bonds at the β C (see Figure 2). The corresponding $P_2(t)$ curves are shown in Figure 3a with half-filled triangles. It can be seen that the relaxation of the C−H bond of the α C is slightly slower than that of the C−H bonds of the β C, and this is attributed to the bulky side group (phenyl ring). However, as we can see from Figure 3a, the difference between the two $P_2(t)$ curves for the C−H bond vectors is very small, leading to almost indistinguishable values for the relaxation times. Therefore, from here on we analyze all C−H bonds of the backbone as a single group. Inspecting the curve, however, it is not at all clear whether this hierarchy of relaxations, which is also found in experiment, only is due to initial fluctuations of different amplitude, leading to lower values of the correlation functions at short times around 100 ps. As mentioned above, the fast initial drop of the C−H vectors is related with very fast local fluctuations of the primitive relaxation at short times. To further explore the slow relaxation process we normalize all the curves of the various bond vectors, shown in Figure 3a, to 1 at 100 ps (see Figure 3b). The question is if the normalized data form a master curve with the same stretching exponent. As we can see from Figure 3b there are still differences, however almost indistinguishable,

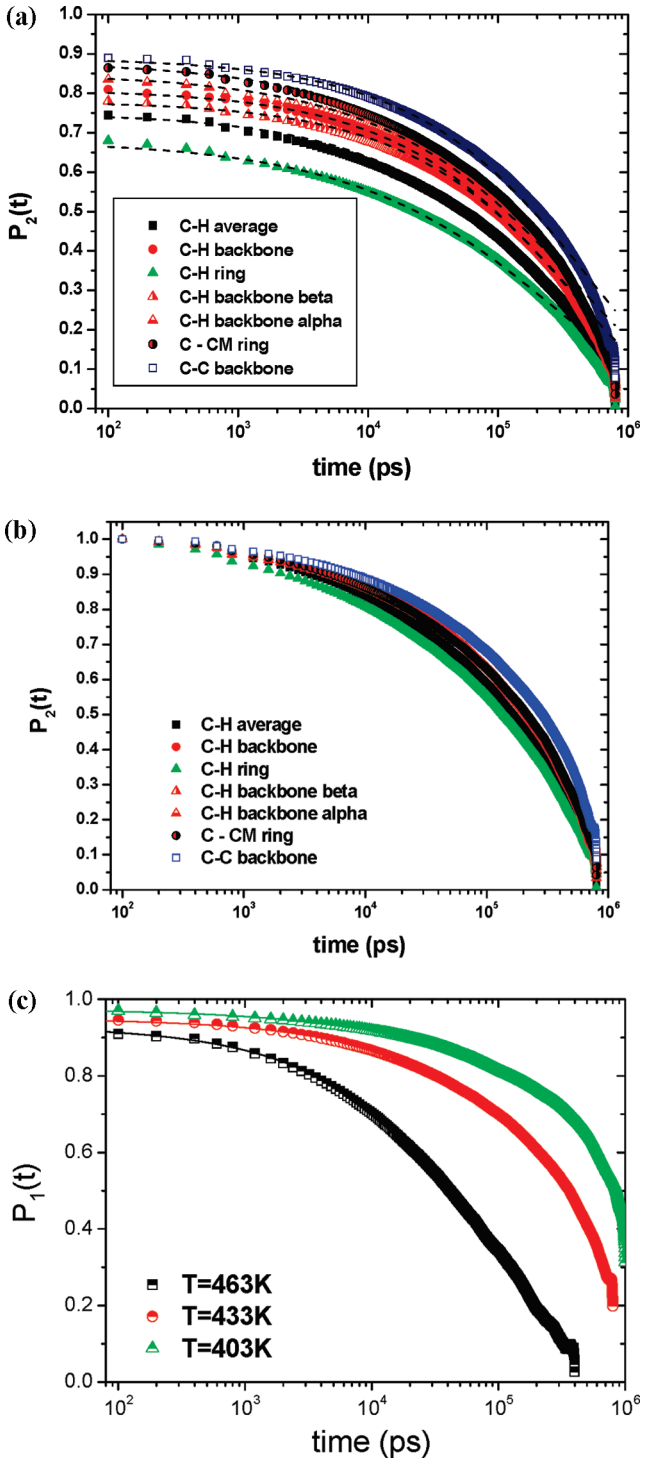

Figure 3. (a) $P_2(t)$ Time-autocorrelation function of various C−H bond vectors, the backbone C−C bond, and the C−CM ring vector at T = 433 K, obtained from the atomistic MD simulations (P = 0.1 MPa). Lines show best KWW fits. (b) $P_2(t)$ Time-autocorrelation function of various C−H bond vectors, the backbone C−C vector, and the C−CM ring bond at T = 433 K, obtained from the atomistic MD simulations (P = 0.1 MPa). Data are scaled in order to start from 1 at t = 100 ps. (c) $P_1(t)$ time-autocorrelation functions of the C−CM ring vector for different temperatures as indicated (P = 0.1 MPa). Lines show best KWW fits.

in the slow relaxation of the different C−H vectors as well as in the stretching exponent (discussed below in Figure 6); thus indicating that the long time decay is governed by the very same structural relaxation processes.

Figure 3c shows the effect of temperature variation (at P = 0.1 MPa) on the P_1 autocorrelation function corresponding to the C−CM ring vector. This quantity is of particular interest here as it is the one that is probed experimentally with DS. $P_1(t)$ exhibits a similar rapid decay at short times as $P_2(t)$, followed by a rather slow decorrelation at later times. Again the short- and long-time regime corresponds to a primitive and to the segmental relaxations, respectively. As expected, the relaxation of the C−CM bonds takes longer with decreasing temperature and at the same time the fast initial decay is smaller due to reduced fluctuations.

It is quite common to fit the long-time regime of such autocorrelation functions by a KWW stretched-exponential function:

$$P_i(t) = A \exp\left[-\left(\frac{t}{\tau_{KWW}}\right)^{\beta}\right], \quad i = 1, 2 \qquad (6)$$

where τ_{KWW} is a characteristic relaxation time, β the stretch exponent, and A a pre-exponential factor that takes into account relaxation processes at very short time scales. The segmental correlation time, τ_s, is defined as the integral of the above equation, which can be numerically calculated. We should also point out here that, in order to examine the fitting procedure, we have used different fitting ranges or even an additional fitting function, including an exponential term for the short-time (up to 10−100 ps) regime. In all cases the differences between the obtained correlation times are 5−10%, i.e., within the error bars. Finally, note that the difference in the calculated relaxation times between the original and the scaled data, shown in Figure 3, parts a and b, respectively, vary only 10−20% due to the difference in the prefactor A. Keeping this in mind, we in the following calculate the segmental relaxation times from the original data, shown in Figure 3a in order to be more consistent with the experimentally available results.

In the next step we compare the segmental relaxation times of the various autocorrelation curves shown in Figure 3,parts a and c. On the basis of the discussion above for the presence of two different modes of decay (a rapid and a slow one), we describe the second regime (times longer than about 10−100 ps) with eq 6. Lines in Figure 3, parts a and c, show the best KWW fits for the $P_2(t)$ and $P_1(t)$ curves, respectively. Values of the pre-exponential factor A were chosen properly to take into account the fast relaxation for the specific T- and P-conditions. Then the relaxation times were calculated from the time integral of $P_1(t)$ or $P_2(t)$. The thus extracted relaxation times are compared in parts a and b of Figure 4. In Figure 4a, the segmental relaxation times of the average C−H bond vector, calculated from the analysis of the $P_1(t)$ and $P_2(t)$ curves as a function of temperature, are shown at atmospheric pressure. At all temperatures, $\tau_1/\tau_2 \cong 2.2-2.7$ (this factor is also similar, within the error bars, for the segmental correlation times of the other vectors studied in this work). Note that according to the Debye theory of rotational relaxation, based upon a simple rotational diffusion coefficient, the ratio of the relaxation times calculated from $P_1(t)$ and $P_2(t)$ curves is $\tau_1/\tau_2 = 3$.[46] Deviations from this theoretical value are associated with the much more complex translational and rotational diffusion of polymeric segments as compared with a simple rotational diffusion.

In Figure 4b segmental relaxation times corresponding to the average C−H bond vector, i.e., all C−H bonds in a PS chain, as well as of individual backbone C−H bonds, ring C−H bonds, the C−CM ring vector, and the terminal relaxation for the three temperatures investigated, are included. Note that the relaxation time of the backbone C−H bonds is consistently

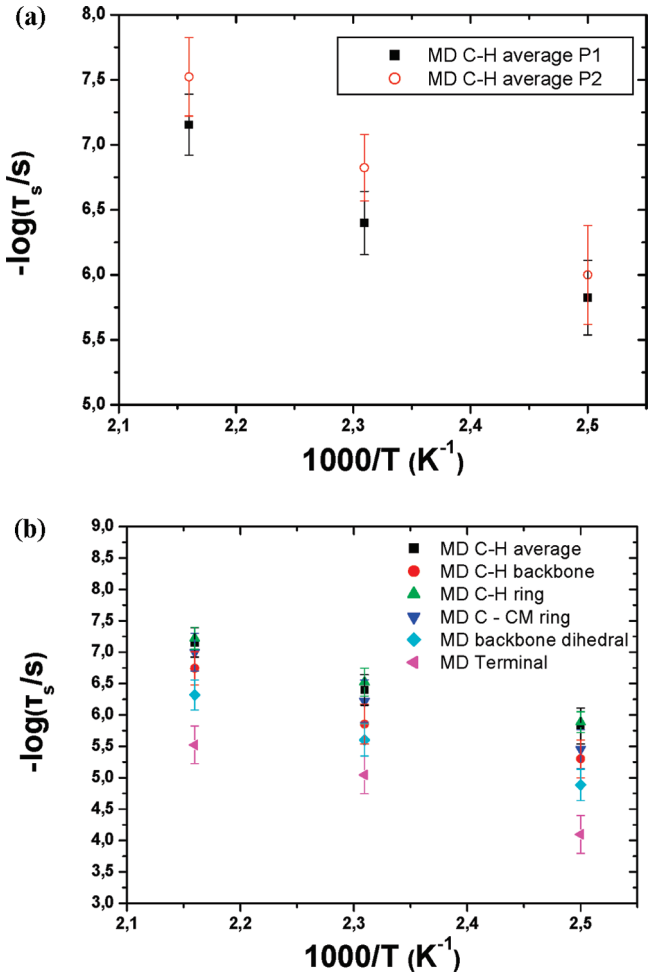

Figure 4. (a) Temperature dependence of the segmental relaxation time obtained through analysis of $P_1(t)$ and $P_2(t)$ curves of the average C−H bond vectors of MD simulation data. (b) Temperature dependence of the different characteristic times obtained through analysis of P_l(t) Legendre polynomials of various vectors of MD simulation data. Data about backbone dihedral relaxation times from the AA MD as well as the maximum (terminal) relaxation time from the CG MD simulations are also shown.

larger than for the ring C−H bonds; their ratio being in the range from 1.5 to 2.

In addition to these local bonds, the local-segmental dynamics of the backbone of PS chains can be also analyzed in the level of the dihedral angle, defined through four consecutive C atoms along the backbone. Dihedral dynamics can be quantified in terms of the torsional autocorrelation function, defined as

$$P(\phi(t)) = \frac{\langle \cos\phi(t)\cos\phi(0)\rangle - \langle\cos\phi(0)\rangle^2}{\langle\cos\phi(0)\cos\phi(0)\rangle - \langle\cos\phi(0)\rangle^2} \qquad (7)$$

where $\phi(t)$ is the dihedral angle at time t. Characteristic dihedral relaxation times can be obtained by fitting P($\phi(t)$) curves with a KWW function and calculating the integral below the curve. Dihedral relaxation times, τ_d, are included in Figure 4b for the different temperatures investigated. Two important conclusions can be derived from these data. First, that the dihedral relaxation times are longer than the C−H ones, at the same temperature and pressure. Indeed, dihedral angles along the backbone decorrelate much slower (about 10 times) than the C−H bonds along the backbone. This is not surprising given that a dihedral angle involves the motion

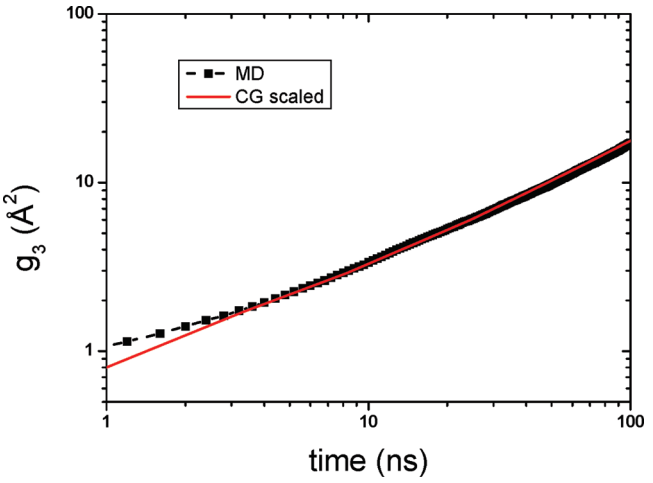

Figure 5. Time scaling of the CG simulations using all-atom data for a PS melt (T = 463 K, P = 1 atm) based on the motion of the center of mass.

of four consecutive carbon atoms. Second, the dihedral relaxation times follow similar temperature dependence as with the relaxation of the C−H bond vectors. This is also the expectation borne out by the fact that all these probes are coupled to the same structural relaxation process.

4.3. Comparison between Simulations and Experiments. In a next step, the chain relaxation of PS has been studied by MD to facilitate a one-to-one comparison with the experimentally measured one (DS and rheology). The long-time chain relaxation of PS chains precludes a prediction through brute force all-atom MD simulations because of the very long relaxation times, especially at the lower temperatures. Therefore, for the chain dynamics we have used a hierarchical scheme that combines atomistic and CG MD simulations. As discussed before, CG MD simulations are much faster than atomistic ones, and the CG time-scale has to be calibrated by all atom simulations or experiment. Through such a time-mapping of CG dynamics on the atomistic one, CG data can be directly compared to experimental or atomistic simulation data.[34] We have followed the above-described procedure in order to calculate the longest relaxation time for the PS chain. Specifically, we determine the time-mapping factor based on mean-square displacement, MSD, of center-of-mass (or of segments) on the atomistic level compared to the CG level. In Figure 5 we show a typical MSD plot for the motion of center-of-mass, $g_3(t) = \langle (R_{cm}(t) - R_{cm}(0))^2 \rangle$, with $\langle\ \rangle$ denoting ensemble average, from atomistic (squares) and CG scaled (line) data, for a specific PS melt (T = 463 K, P = 1 atm). As we can see, the agreement between the two sets of data is excellent for all times above about 300 ps and lengths of a few Å. Next, all CG dynamic quantities for this specific system are scaled to this factor. Qualitatively similar is the situation for different T, P conditions. Note that as we show elsewhere the scaling factor is the same if the MSD of center-of-mass or of the individual beads is used.[34]

Subsequently, the autocorrelation factor of the first normal mode is described by the KWW function that provides with the maximum (Rouse) relaxation time, τ_R, for the PS chain.[2,20] The thus obtained, τ_R, from the CG MD simulations are included in Figure 4b. Within the investigated temperature range, τ_R has a similar temperature dependence with the segmental relaxation times. Furthermore, τ_R is, as expected, larger than the dihedral relaxation time by a factor of 3−5. The reason is the rather short chain length, i.e., a 18mer PS consists of only 36 backbone atoms.

The thus obtained MD relaxation times can now be compared to the experimental ones. On the experimental

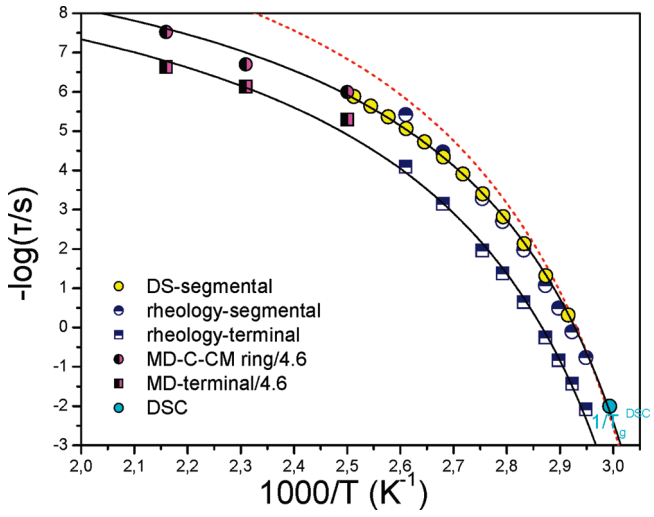

Figure 6. Compilation of the relaxation times through MD corresponding to the C−CM ring vector (vertical half-filled symbols), DS (filled circles in yellow), DSC at τ = 100 s (filled circle in blue) and rheology (horizontal half-filled symbols) at the different temperatures investigated. The latter times were scaled to the DS and DSC T_g (see text). The MD and DS times correspond to the $P_1(t)$ time-autocorrelation functions (see text). Only the segmental (circles) and the terminal (squares) relaxation times are shown. The solid lines are the result of the fit to the VFT equation. The dashed line is the T_g-scaled VFT obtained by NMR.

side, rheology provides with both the segmental and terminal times. The frequency scale shift factor, a_T, was applied to the master-curve (Figure S2, Supporting Information), resulting to the T-dependence of the two characteristic frequencies, ω_S and ω_c, corresponding to the segmental and chain dynamics, respectively. These frequencies correspond to the crossing of the storage and loss moduli (ω_S) and to the crossing of lines with slopes 2 and 1, respectively (ω_c) corresponding to the terminal regime. The dynamics extracted from rheology is compared to the one from DS and the simulations in Figure 6. First, in comparing the rheology and dielectric times we find that the crossing of the storage and loss moduli for the segmental relaxation process (Figure S2, Supporting Information) occurs at lower frequencies as compared to the dielectric loss maximum. Parenthetically, the electric modulus representation, $M^*(\omega) = 1/\varepsilon^*(\omega)$, is more suitable when comparing rheology with DS relaxation times, however, the low dielectric activity of PS makes the peak frequency in ε'' and M'' nearly indistinguishable. Thus, the reason for the faster segmental dynamics as probed by rheology is not the different representation. This suggests that for PS, dynamic mechanical and dielectric spectroscopies, performed on the same sample, are sensitive to different kinds of motion. Indeed, dielectric relaxation is probing the response of the dipolar units to the external electric field whereas rheology is affected by the way the underlying molecular motion couples to the applied stress. Thus, the two times need not be the same.

Since the purpose of the present investigation is to make a one-to-one comparison of the dipolar relaxation being perpendicular to the backbone with the relaxation of the C−CM vector obtained in MD, in Figure 6 the rheology times have been scaled to the DS and DSC T_g. This facilitates the comparison with the terminal dynamics as studied by MD (the latter for the C−CM ring autocorrelation function) and rheology. The Figure includes the DSC glass temperature (assuming isochronal at $\tau\sim$100 s). We found that the MD relaxation times, using the $P_1(t)$ curves, follow qualitatively very well the temperature dependence found by DS (again $P_1(t)$) but a quantitative comparison reveals that MD relaxation times are slower than DS by a factor of about 4.6. This discrepancy can have different origins. First, the molecular weights of the sample used in MD and DS are not identical. An 18mer has a somewhat larger molecular weight that the one investigated experimentally, and to the extent that the segmental dynamics are influenced by the mobile chain-ends this can result in faster experimental dynamics. The Rouse times (relaxation time of the first normal mode) would deviate by a factor of about almost 1.4. In addition the natural abundance of very short fragments in polydisperse samples leads to larger local mobilities. The effect of the different molecular weight and of polydispersity will be a subject of a future work. Second, the all-atom model, used in this work, has been developed[38] through parametrization of (a) quantum calculations of very small fragments (the intramolecular bonded interactions) and (b) fittings of the intermolecular nonbonded interactions in order to reproduce the experimental density (at 1 atm) and heat of vaporization of liquid benzene. If we consider the difference between the density values of the *NPT* MD PS simulations and experimental data (density by the AA force field is about 3−4% larger than the experimental one) then it seems that the latter procedure, i.e. the extension of the benzene nonbonded interaction parameters to PS melts, is the most problematic one. In order to test this hypothesis we have performed a few test atomistic NPT MD runs, with a modified all-atom model in which the minimum of the cohesive intermolecular energy between all atoms (the corresponding ε_C, and ε_H in the Lennard-Jones parameters) were decreased about 15%, in order the density of the NPT MD simulations of the PS 18mer system to match the experimental density (at 1 atm). This result, as expected, into faster segmental relaxation times of about 3 times, thus the new MD relaxation times, are slower than the DS with a factor of only 1.5, which compares well to the one expected from the different chain lengths. However, since we do not have any solid basis on the physical reason for the modified all-atom model and the goal of the present work is not to develop a new all-atom PS force field, we decide here to report data from the original atomistic model. In overall, taken into account the approximations of such parametrizations in atomistic force fields, and also that there is no adjustment of the model to any dynamical quantity, it is not surprising that the MD relaxation times are somewhat larger than the experimental times and the agreement, and here especially the temperature dependence is very good. Lastly, the experimental times are influenced by the strong ionic conductivity, due to impurities—a dynamic process that is not affecting MD—and thus cause also some uncertainty to the experiment (about the symbol size). Nevertheless, this factor seems to be independent of temperature and pressure. Therefore, we present the MD data here scaled by this factor. This facilitates the comparison of terminal relaxation times obtained from rheology with the longest Rouse time obtained from MD simulations. The nonscaled MD data can be found in the Supporting Information (Figure S3).

The temperature dependence of both time-scales can also be described by the Vogel−Fulcher−Tammann (VFT) equation:

$$\tau_c = \tau_o \exp\left(\frac{B}{T - T_0}\right) \tag{8}$$

where τ_0 is the relaxation time calibration constant in the limit of very high temperatures, B is a generalized activation energy and T_0 is the Vogel temperature known as the "ideal" glass temperature "zero temperature" where all relaxation times diverge. The combined DSC, DS, rheology and MD data for the segmental process result to $\tau_0 = (5 \pm 2)\text{x}10^{-11}$s, B = 1040 ± 80 K and T_0 = 298 ± 2 K. These parameters are somewhat different than the ones obtained earlier for the segmental relaxation of atactic PS (M = 2100g/mol) through various NMR experiments and MD simulations covering a broad T-range from 390 to 510 K[17]

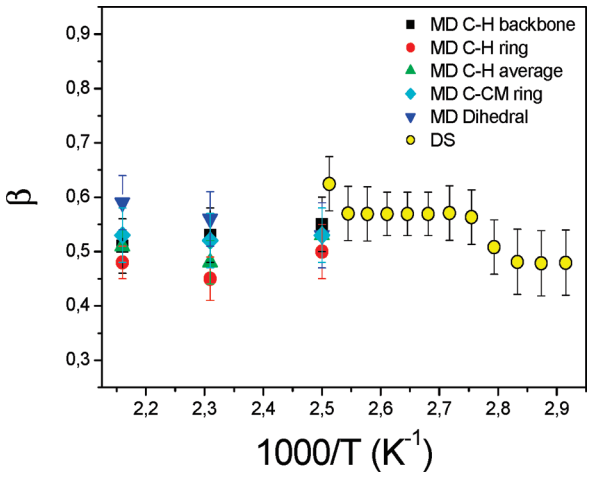

Figure 7. KWW stretch exponent, β, obtained through the different $P_1(t)$ curves (MD) and calculated in DS plotted as a function of temperature.

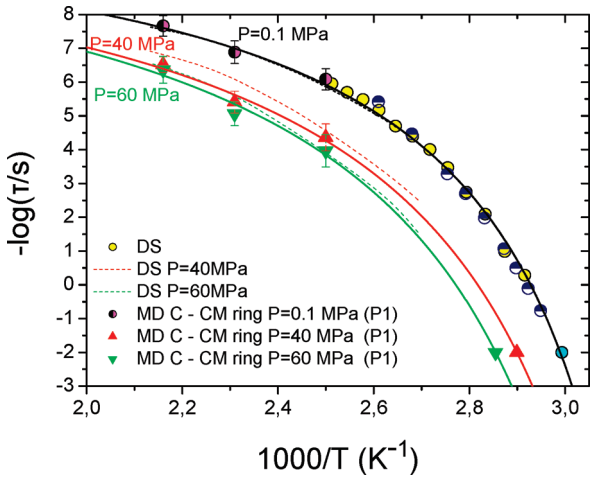

Figure 8. Pressure dependence of the segmental relaxation times obtained from MD (C−CM ring vector) at 0.1, 40, and 60 MPa. The different symbols for the relaxation times at 0.1 MPa are the same as in Figure 6. The points at τ = 100s are obtained through *PVT* (by assuming that the glass temperature is isochronal). The solid lines are the result of the fit to the VFT equation. The dashed black, red and green lines are literature[42] T_g-scaled dielectric relaxation times measured at 0.1 MPa and calculated at 40 and 60 MPa, respectively.

(shown by the dotted line in Figure 6). The latter times are faster on the high temperature side (the NMR times were scaled to the current T_g), but this is not surprising given that they present $P_2(t)$ correlation times ($\tau_2 \sim \tau_1/3$). On the other hand, the combined data for the terminal relaxation (rheology, MD) result to very similar values: $\tau_0 = (2 \pm 1) \times 10^{-10}$ s, $B = 1150 \pm 20$ K, and $T_0 = 298 \pm 2$ K. We are aware that higher molecular weight polymers, show different T-dependencies for the segmental and terminal relaxations in the vicinity of T_g.[47−50] This is not evident here, probably because of the low molecular weight.

In Figure 7, the KWW exponent, β, of the different autocorrelation functions is plotted as a function of temperature and compared with the one obtained experimentally (DS). In all cases, β is considerably lower than 1, thus indicating a broad distribution of relaxation times. The KWW exponent of the autocorrelation function for the C−H bonds, β_{C-H}, varies between 0.45 to 0.55. The stretching exponent is independent of temperature. The C−CM ring values are also in very good agreement with β_{DS}, the latter extracted from the HN shape parameters as described earlier. The β_{C-H} values depend only slightly on the position of the C−H bonds, being somewhat the β_{C-H} values for the backbone C−H bonds. The latter could be attributed to the additional relaxation mechanism of the C−H bonds in the phenyl ring, related with the orientational motion of the ring. Values for the KWW exponent of the dihedral autocorrelation function, β_d, vary between 0.5 and 0.6, being higher than the β_{C-H} ones. This is not surprising, since for the C−H bonds additional relaxation mechanisms (such as bond vibrations, angle librations, phenyl ring motions) play a more significant role than for the relaxation of the backbone dihedral leading to a broader distribution of relaxation times. Furthermore, there seems to be a weak dependence of β_d on temperature; i.e., β_d decreases with decreasing temperature. Note also the large error bars of the β values, especially at lower temperatures, due to limited time-window available. Finally it should be stated, that values of both β_{C-H} and β_d presented here are typical for amorphous polymers and in agreement with data reported in the literature by other MD simulations of polystyrene[15,26,27] and other polymers like polyethylene[12,20] and polybutadiene.[22]

4.4. Pressure Dependence of Segmental Dynamics. In this section we present the first results on the effect of pressure on the segmental dynamics of PS by means of MD simulations, performed at experimental density (see Figure 1) at two elevated pressures (40 and 60 MPa). Computationally, this is not a trivial task since at elevated pressures the segmental dynamics are slowed-down as a result of densification. In addition, the presence of higher conductivity makes pressure-dependent DS measurements a difficult task for this sample. To overcome these problems we use a combination of experimental *PVT* $T_g(P)$ dependencies (Figure 1) together with the simulation data at two pressures, 40 and 60 MPa.

As mentioned above the $P_2(t)$ autocorrelation curves of various C−H bond vectors as well as the C−CM ring vector at elevated pressures show the same structure as the curves at the atmospheric pressure, discussed in section 4.2. In Figure S4 (Supporting Information), we present such curves for the C−CM ring vector at T = 463 K. From these curves the relaxation times at elevated pressures can be calculated following the analysis presented before (see section 4.2). In Figure 8 the segmental relaxation times obtained through the all-atom MD simulations are shown together with the *PVT* times (the assumption here is that T_g is "isochronal" at 100 s). As expected, increasing pressure slows-down the segmental dynamics and increases the glass temperature. Despite the few experimental points, the MD and *PVT* $\tau(T)$ data span more than 8 orders of magnitude.

The combined $\tau(T)$ times at elevated pressures are described by the same VFT equation for the different isobars (shown in Figure 8 with the solid lines). In addition, we display literature[42] DS segmental relaxation times at elevated pressures from a PS with M_w = 780 g/mol. Following a T_g-scaling of the dynamics to account for the difference in molecular weights the interpolated segmental relaxation times at the investigated pressures are also shown in Figure 8 with the dashed lines. Note that there is a near quantitative agreement between the MD simulation and DS results.

Segmental relaxation times calculated from the VFT parameters at different temperatures and pressures are shown in Figure 9. Intrinsic to the pressure dependence of segmental relaxation times is information that relates to the apparent activation volume.[51] The latter quantity, $\Delta V^{\ddagger} = 2.303RT(\partial[\log \tau]/\partial P)_T$), represents the pressure sensitivity of the segmental relaxation times and was originally interpreted as reflecting the difference in molar volumes of activated and nonactivated species.[52,53,54] $\Delta V^{\ddagger}$ can be extracted from the slopes of the "isothermal"

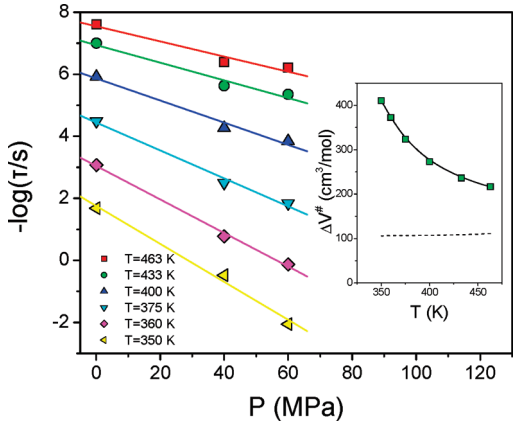

Figure 9. Pressure dependence of the segmental relaxation times calculated from the VFT parameters at different temperatures as indicated. In the inset, the apparent activation volume is obtained and plotted as a function of temperature. The dashed line is the monomer volume.

representation (inset to Figure 9). Several experimental studies[45,47,55,56] on glass-forming systems probed the temperature dependence of the apparent activation volume; $\Delta V^{\ddagger}$ has a strong T-dependence, increasing by decreasing temperature toward the glass temperature. At the same time the high temperature values of $\Delta V^{\ddagger}$ approach the monomer volume at some 70−100 K above the glass temperature. In the inset of Figure 9 the monomer volume, in cm^3/mol (calculated from the PVT density data of Figure 1), is shown with dash line for all temperatures studied here (at P = 0.1 MPa). Herein the obtained values do show the expected increase at lower temperatures, but the limiting values at higher temperatures are still above the monomer volume, probably because of the limited accuracy of the VFT parameters.

5. Conclusions

The segmental and terminal dynamics of a-PS have been investigated by hierarchical simulation methodologies and experiments at atmospheric and, for the first time, at elevated pressures. We have examined the polymer dynamics both at the submonomer and end-to-end distance level using a multiscale simulation approach that combines atomistic and coarse-grained dynamic simulations. We have also presented, for the first time, an investigation of the atactic PS dynamics as a function of pressure.

The detailed, all-atom MD simulations at atmospheric pressure, revealed that the various characteristic times corresponding to the decay of time-autocorrelation functions for various C−H bond vectors as well as of the C−CM ring bond can be different by nearly one decade but all share the same temperature dependence and have nearly the same distribution of relaxation times that is in agreement with the one obtained through dielectric spectroscopy. When the $P_1(t)$ times for the relevant C−CM ring bond were compared to the dipolar dynamics obtained though dielectric spectroscopy they were found to be slower by a factor of about 4.6. That could be accounted for by various factors, involving differences between PS model systems and experimental samples as well as approximations in the parametrization of the atomistic force field. When the MD data were scaled by this factor toward the DS times, the predicted terminal dynamics were in excellent agreement with the ones obtained by rheology.

MD simulations were also performed at elevated pressures using the experimental equation-of-state as a guide. As expected, as the pressure increases the segmental dynamics slows-down and the glass temperature increases. The obtained temperature dependence of relaxation times and the associated glass temperatures at the two elevated pressures investigated were also found to be in good agreement with the experimentally measured glass temperature and allowed extracting the apparent activation volume as a function of temperature.

Acknowledgment. We thank H. W. Spiess, B. Dünweg and D. Fritz for helpful discussions. We thank A. Best and A. Hanewald for the PVT and rheology measurement, respectively.

Supporting Information Available: Plots of dielectric loss spectra, storage and loss shear moduli, compilation of the relaxation times, and $P_2(t)$ time-autocorrelation functions. This material is available free of charge via the Internet at http://pubs.acs.org.

References and Notes

(1) Ferry, J. D. *Viscoelastic Properties of Polymers*; John Wiley and Sons: New York, 1980.
(2) Doi, M.; Edwards, S. F. *The Theory of Polymer Dynamics*; Claredon Press: Oxford, England, 1986.
(3) *Simulation Methods for Polymers*; Theodorou, D. N., Kotelyanski, M., Eds.; Marcel Dekker: New York, 2004.
(4) Baschnagel, J.; Binder, K.; Doruker, P.; Gusev, A. A.; Hahn, O.; Kremer, K.; Mattice, W. L.; Müller-Plathe, F.; Murat, M.; Paul, W.; Santos, S.; Suter, U. W.; Tries, V. *Adv. Polym. Sci.* **2000**, *152*, 41.
(5) Kremer, K.; Peter, C. *Faraday Discuss.* **2010**, *144*, 9.
(6) Floudas, G.; Mpoukouvalas, K.; Papadopoulos, P. *J. Chem. Phys.* **2006**, *124*, 074905.
(7) Tölle, A.; Schober, H.; Wuttke, J.; Randl, O. G.; Fujara, F. *Phys. Rev. Lett.* **1998**, *80*, 2374.
(8) Dreyfus, C.; Aouadi, A.; Gapinski, J.; Matos-Lopes, M.; Steffen, W.; Patkowski, A.; Pick, R. M. *Phys. Rev. E* **2003**, *68*, 011204.
(9) Casalini, R.; Roland, C. M. *Phys. Rev. E* **2004**, *69*, 062501.
(10) Alba-Simionseco, C.; Cailliaux, A.; Alegria, A.; Tarjus, G. *Europhys. Lett.* **2004**, *68*, 58.
(11) Roland, C. M.; Hensel-Bielowka, S.; Paluch, M.; Casalini, R. *Rep. Prog. Phys.* **2005**, *68*, 1405.
(12) Pant, P. V. K.; Han, J.; Smith, G. D.; Boyd, R. H. *J. Chem. Phys.* **1993**, *99*, 597.
(13) Bharadwaj, R. K.; Boyd, R. H. *Macromolecules* **2000**, *33*, 5897.
(14) Hotston, S. D.; Adolf, D. B.; Karatasos, K. *J. Chem. Phys.* **2001**, *115*, 2359.
(15) Smith, G. D.; Borodin, O.; Bedrov, D.; Paul, W.; Qiu, X. H.; Ediger, M. D. *Macromolecules* **2001**, *34*, 5192.
(16) Smith, G. D.; Borodin, O.; Paul, W. *J. Chem. Phys.* **2002**, *117*, 10350.
(17) He, Y.; Lutz, T. R.; Ediger, M. D.; Ayyagari, C.; Bedrov, D.; Smith, G. D. *Macromolecules* **2004**, *37*, 5032.
(18) Yang, L.; Srolovitz, D. J.; Yee, A. F. *J. Chem. Phys.* **1999**, *110*, 7058.
(19) Qiu, X.; Ediger, M. D. *Macromolecules* **2000**, 490.
(20) Harmandaris, V. A.; Mavrantzas, V. G.; Theodorou, D. N. *Macromolecules* **1998**, *31*, 7934. Harmandaris, V. A.; Mavrantzas, V. G.; Theodorou, D. N.; Kroeger, M.; Ramirej, J. O.; Oettinger, H. C.; Vlassopoulos, D. *Macromolecules* **2003**, *36*, 1376.
(21) Ahumada, O.; Theodorou, D. N.; Triolo, A.; Arrighi, V.; Karatasos, C.; Ryckaert, J. P. *Macromolecules* **2002**, *35*, 7110.
(22) Tsolou, G.; Harmandaris, V. A.; Mavrantzas, V. G. *J. Chem. Phys.* **2006**, *124*, 084906. Tsolou, G.; Harmandaris, V. A.; Mavrantzas, V. G. *Macromol. Theor. Simul.* **2006**, *15*, 381. Tsolou, G.; Harmandaris, V. A.; Mavrantzas, V. G. *J. Non-Newtonian Fluid Dyn.* **2008**, *152*, 184.
(23) Kirpatch, A.; Adolf, D. B. *Macromolecules* **2004**, *37*, 1576.
(24) Faller, R.; Müller-Plathe, F.; Doxastakis, M.; Theodorou, D. *Macromolecules* **2001**, *34*, 1436.
(25) Doxastakis, M.; Theodorou, D. N.; Fytas, G.; Kremer, F.; Faller, R.; Müller-Plathe, F.; Hadjichristidis, N. *J. Chem. Phys.* **2003**, *119*, 6883.
(26) Lyulin, A. V.; Michels, M. A. *J. Comput. Phys. Commun.* **2002**, *147*, 298. *Macromolecules* **2002**, *35*, 1463.
(27) Vorselaars, B.; Lyulin, A. V.; Michels, M. A. *Macromolecules* **2007**, *40*, 6001.
(28) Liu, J.; Wu, S.; Cao, D.; Zhang, L. *J. Chem. Phys.* **2008**, *129*, 154905.
(29) Kremer, K.; Grest, G. *J. Chem. Phys.* **1990**, *92*, 5097. León, S.; Van der Vegt, N.; Delle Site, L.; Kremer, K. *Macromolecules* **2005**, *38*, 8078.

(30) Bennemann, C.; Paul, W.; Baschnagel, J.; Binder, K. *J. Phys.: Condens. Matter* **1999**, *11*, 2179.
(31) Barbieri, A.; Prevosto, D.; Lucchesi, M.; Leporini, D. *J. Phys.: Condens. Matter* **2004**, *16*, 6609.
(32) Tschöp, W.; Kremer, K.; Batoulis, J.; Buerger, T.; Hahn, O. *Acta Polym.* **1998**, *49*, 61. **1998**, *49*, 75.
(33) Harmandaris, V. A.; Reith, D.; Van der Vegt, N. F. A.; Kremer, K. *Macromol. Chem. Phys.* **2007**, *208*, 2109. Harmandaris, V. A.; Adhikari, N. P.; Van der Vegt, N. F. A.; Kremer, K.; Mann, B. A.; Voelkel, R.; Weiss, H.; Liew, CheeChin. *Macromolecules* **2007**, *40*, 7026.
(34) Harmandaris, V. A.; Kremer, K. *Macromolecules* **2009**, *42*, 791. Harmandaris, V. A.; Kremer, K. *Soft Matter* **2009**, *5*, 3920.
(35) Fritz, D.; Harmandaris, V. A.; Kremer, K.; Van der Vegt, N. F. A. *Macromolecules* **2009**, *42*, 7579.
(36) *Broadband Dielectric Spectroscopy*; Kremer, F., Schönhals, A., Eds; Spinger: Berlin, 2002.
(37) Alvarez, F.; Alegria, A.; Colmenero, J. *Phys. Rev. B.* **1991**, *44*, 7306.
(38) Müller-Plathe, F. *Macromolecules* **1996**, *29*, 4782.
(39) Hess, B.; Kutzner, C.; van der Spoel, D.; Lindahl, E. *J. Chem. Theor. Comput.* **2008**, *4*, 435–447.
(40) Baig, C.; Harmandaris, V. A. *Macromolecules* **2010**, *43*, 3156.
(41) Limbach, H. J.; Arnold, A.; Mann, B. A.; Holm, C. *Comput. Phys. Commun.* **2006**, *174*, 704; see also: http://www.espresso.mpg.de/.
(42) Schwartz, G. A.; Colmenero, J.; Alegria, A. *J. Non-Cryst. Solids* **2007**, *353*, 4298.
(43) Simon, F. E.; Glatzel, Z. *Z. Anorg. Allg. Chem.* **1929**, *178*, 309.
(44) Andresson, S. P.; Andersson, O. *Macromolecules* **1998**, *31*, 2992.
(45) Gitsas, A.; Floudas, G. *Macromolecules* **2008**, *41*, 9423.
(46) McQuarie, D. A. *Statistical Mechanics*; University Science Books: New York, 2000.
(47) Mpoukouvalas, K.; Gomopoulos, N.; Floudas, G.; Herrmann, C.; Hanewald, A.; Best, A. *Polymer* **2006**, *47*, 7170.
(48) Plazek, D. J.; Schlosser, E.; Schönhals, A.; Ngai, K. L. *J. Chem. Phys.* **1993**, *98*, 6488.
(49) Schönhals, A. *Macromolecules* **1993**, *26*, 1309.
(50) Nicolai, T.; Floudas, G. *Macromolecules* **1998**, *31*, 2578.
(51) Floudas, G.; Reisinger, T. *J. Chem. Phys.* **1999**, *111*, 5201.
(52) Floudas, G. In *Broadband Dielectric Spectroscopy*; Kremer, F., Schönhals, A.; Eds.; Springer: Berlin, 2002.
(53) Glasstone, S. T., Leidler, K. J., Eyring, H. *Theory of rate process* McGraw-Hill: New York, 1941.
(54) Williams, G. *Trans. Faraday Soc.* **1964**, *60*, 1548.
(55) Floudas, G.; Gravalides, C.; Reisinger, T.; Wegner, G. *J. Chem. Phys.* **1999**, *111*, 9847.
(56) Mpoukouvalas, K.; Floudas, G.; Williams, G. *Macromolecules* **2009**, *42*, 4690.